Cume 399, September 12, 2015, by R. Walterbos

This cume is based on the paper "ALMA Observations of 99GHz free-free and H α 40 line emission from star formation in the centre of NGC 253", published in MNRAS, 450, L80, 2015, by Bendo et al.

Attached is a sheet with physical constants. You may use your calculator but not any stored formulas it may have.

Each (sub)question is worth 5 points for a total of 65 points. Expected passing grade is around 70%.

- 1. Section 2 of the paper describes the data.
 - a. Show how the channel width of 1.5 km/s follows from the information stated on page 2.

This follows from the frequency width of one channel compared to the central frequency, using the Doppler formula.

b. The data includes observations of a flux calibrator, a band-pass calibrator, and a phase calibrator. Describe in a few lines for each of these what their purpose is.

A flux calibrator is necessary to calibrate the flux scale of the measurements, the band-pass calibrator is required because they use a wide band-pass with many channels and to remove any instrumental effects, the shape of that band-pass needs to be calibrated to avoid spurious peaks or ripples in the spectrum. The phase calibrator is required to correct for phase errors in the observations. Phase errors would lead to positional inaccuracies and a "dirty beam shape" for the data that would not match the synthesized beam. If that is the case, cleaning the data would fail and the observations would not reach the theoretical noise levels possible.

c. What is the field of view of the ALMA array for a single pointing at a frequency of 98 GHz? What sets the field of view? Show how to calculate it.

The primary beam of a single dish in the array, at the frequency of observation, sets the field of view for the array. It is equal to $1.2\lambda/D$, where D is the diameter of a single dish.

d. The text quotes a distance of 3.44 Mpc. What does 1arcsec correspond to in pc at this distance? Show the calculation.

Straightforward small angle calculation.

e. What is meant with the "reconstructed beam"? Why is it necessary? (Hint: it is also called the "clean beam" and is hence related to the CLEAN process on interferometer data.)

The data need to be cleaned to remove the effects of all the missing spacings or baselines in the interferometer data. These produce grating rings and missing flux. Cleaning allows for recovery of missing flux and and a cleaner view of the actual intensity distribution. The reconstructed beam is usually the central part of the synthesized beam. The clean beam is convolved with the delta function "clean peaks" found in the CLEAN process, to arrive at the final map.

f. The authors state on page 2, right column: "...we lack the uv coverage to recover >20 arcsec structures". What is meant with "uv coverage"? Why are they not sensitive to structures larger than 20 arcsec? How would we calculate the largest structure an interferometer can see?

Due to missing spacings at short baselines an interferometer cannot see structures larger than a certain angular size. The dimension of that size is set by the shortest baselines observed. The angular size of the largest structure is approximately equal to λ/D radians where D is the shortest baseline observed.

- 2. This problem deals with some of the basics of one observational tracer used in the paper.
 - a. What is a recombination line? In which astrophysical situations does it occur?

A recombination occurs when a proton or ion recombines with an electron. This will happen continuously in ionized plasmas. The line is a bound-bound transition following an initial free-bound capture of the electron. The electron will cascade down to ground level in the ISM emitting various recombination lines in the process.

b. The paper gives the frequency of the H40 α line. Verify this frequency, using the Bohr model for the Hydrogen atom. You may recall that for the optical H α line the wavelength is 6562.8 Å. This line would be written as "H2 α " if we were to use the equivalent notation as used for H40 α . You can use this information to figure out what the electron levels are that are involved in the H40 α transition and the Bohr model energy level dependence on principal quantum number n to get to the frequency of the H40 α line.

This H α line is the 3 to 2 transition. The H40 α line is the 41 to 40 transition. The Bohr model states that levels are separated by $1/n^2 - 1/(n+1)^2$. This can be used to calculate the frequency from the known H α wavelength.

- 3. In section 3, the authors analyze the continuum emission. A question they address is if the origin of the 99GHz is "thermal emission" or a combination of emission processes.
 - a. Which three continuum emission processes can contribute and what do they conclude about the origin of the 99 GHz emission? Describe the physical process for each of the three radiation mechanisms.

This is discussed in Figure 3, so the students mostly have to read the paper carefully. The processes are synchrotron, free-free, and dust continuum emission.

b. If the continuum emission in the ALMA observations is mostly thermal emission, why is it related to the H40 α recombination line? I don't need an explanation of the formula, but I would like you to explain in words why the two emission processes are physically related.

In an HII region the free-free emission is directly related to the recombination line emission because both processes are controlled by electron-ion encounters. There is some dependence on temperature but at a particular temperature the ratio of the two emissivities is a constant.

c. Why can the $H40\alpha$ line emission and the thermal continuum be used as measurements of star formation? What is the physical connection between star formation and this emission?

Massive stars ionize the gas, and by observing the emission from the ionized gas we are essentially counting ionizing photons, since there is an equilibrium between ionization and recombination. Since massive stars have short lives, the presence of HII regions is a measure of the current rate of massive star formation. By extrapolating using an initial mass function over the entire range of stellar masses we can derive a total SFR.

d. The caption for Figure 3 discusses a "modified Rayleigh-Jeans function" for the blue line in Figure 3. If the Rayleigh Jeans function were not modified, what would the slope have been? (Hint: "modified" refers here to a modified Planck intensity spectrum. So if we don't modify the Planck spectrum, what is the slope?)

The slope would be 2, as immediately follows from the RJ approximation for a black body (i.e. Planck) function.

e Speed of light in vacuum $h=2\pi h$ Planck's constant $h=h/2\pi$ Rationalized Planck's constant $h=h/2\pi$ Elementary charge of an electron $h=h/2\pi$ Avogadro's number $h=h/2\pi$ Avogadro's number $h=h/2\pi$ Atomic mass unit $h=h/2\pi$ Atomic mass unit $h=h/2\pi$ Electron charge to mass ratio $h=h/2\pi$ Rationalized $h=h/2\pi$ Rationalized $h=h/2\pi$ Compton wavelength $h=h/2\pi$ Classical electron radius $h=h/2\pi$ Classical	2.997924562(11) × 10^{10} cm s ⁻¹ 6.626196(50) × 10^{-27} erg s 1.0545919(80) × 10^{-27} erg s 1.380622(59) × 10^{-16} erg K ⁻¹ 4.803250(21) × 10^{-10} esu 9.109558(54) × 10^{-28} g 6.6732(31) × 10^{-8} dyn cm ² g ⁻² 6.022169(40) × 10^{23} mole ⁻¹ 1.660531(11) × 10^{-24} g 7.297351(11) × 10^{-3} 5.272759(16) × 10^{17} esu g ⁻¹ 1.09737312(11) × 10^{5} cm ⁻¹ 5.2917715(81) × 10^{-9} cm 2.4263096(74) × 10^{-10} cm 2.817939(13) × 10^{-13} cm 8.31434(35) × 10^{7} erg K ⁻¹ mole ⁻¹ 5.66961(96) × 10^{-5} erg cm ⁻² s ⁻¹ K ⁻⁴ 6.652453(62) × 10^{-25} cm ² 1.49597892(1) × 10^{13} cm 3.0856(1) × 10^{18} cm 9.4605 × 10^{17} cm = 6.324 × 10^{4} a. u. 1.989(2) × 10^{33} g 6.9598(7) × 10^{10} cm

Symbol	Meaning				
	Solar luminosity	$3.826(8) \times 10^{33} \text{ erg s}^{-1}$			
L _⊙ 1 e.V.	One electron volt associated wavelength associated wavenumber associated frequency associated energy	12,396.3 × 10 ⁻⁸ cm 8067.1 cm ⁻¹ 2.41838 × 10 ¹⁴ Hz 1.60184 × 10 ⁻¹² erg 11,605.9 °K			

Value

ALMA observations of 99 GHz free–free and H40 α line emission from star formation in the centre of NGC 253

G. J. Bendo, 1,2

R. J. Beswick, 1,2 M. J. D'Cruze, 1 C. Dickinson, 1 G. A. Fuller 1,2 and T. W. B. Muxlow 1,2

⁴ Jodrell Bank Centre for Astrophysics, School of Physics and Astronomy, The University of Manchester, Oxford Road, Manchester M13 9PL, UK ²UK ALMA Regional Centre Nade

Accepted 2015 April 7. Received 2015 April 6; in original form 2015 January 21

ABSTRACT

We present Atacama Large Millimeter/submillimeter Array observations of 99.02 GHz free-free and H40 α emission from the centre of the nearby starburst galaxy NGC 253. We calculate electron temperatures of 3700–4500 K for the photoionized gas, which agrees with previous measurements. We measure a photoionizing photon production rate of (3.2 \pm 0.2) \times 10⁵³ s⁻¹ and a star formation rate of 1.73 \pm 0.12 M $_{\odot}$ yr⁻¹ within the central 20 \times 10 arcsec, which fall within the broad range of measurements from previous millimetre and radio observations but which are better constrained. We also demonstrate that the dust opacities are \sim 3 dex higher than inferred from previous near-infrared data, which illustrates the benefits of using millimetre star formation tracers in very dusty sources.

Key words: galaxies: individual: NGC 253 – galaxies: starburst – radio continuum: galaxies – radio lines: galaxies.

1 INTRODUCTION

The millimetre waveband contains two star formation tracers that directly trace photoionizing light from star-forming regions while not suffering from dust obscuration effects, making it a superior alternative to star formation tracers in other wavebands (see Calzetti et al. 2009 and Murphy et al. 2011 for reviews). The continuum emission includes free-free emission, and while thermal dust emission is dominant at >100 GHz and synchrotron emission is more prominent at ≤30 GHz, free-free emission is the dominant emission source at 30–100 GHz (e.g. Peel et al. 2011). Multiple hydrogen recombination lines are seen at millimetre wavelengths as well. Optical and near-infrared lines are affected by dust extinction effects, and centimetre and metre recombination lines are affected by potential masing and collisional broadening effects, but millimetre lines are not affected by any of these problems (e.g. Gordon & Walmsley 1990) and are therefore more accurate tracers of star formation.

The Atacama Large Millimeter/submillimeter Array (ALMA) is a groundbreaking millimetre and submillimetre telescope with the capability of reaching sensitivity levels in the 30-950 GHz range at least an order of magnitude better than other telescopes (see Lundgren 2013 for a technical overview). ALMA is capable of detecting free-free and recombination line emission from many nearby infrared-luminous galaxies (Scoville & Murchikova 2013).

It is therefore of interest to use early ALMA observations to explore the telescope's capabilities to detect these star formation tracers.

In this paper, we present ALMA observations of free-free continuum emission and H40 α emission at 99.02 GHz from the centre of NGC 253 that we use to derive star formation rates (SFRs) as well as the electron temperature (T_e) of the gas. In addition, we use the H40 α data together with near-infrared data from Engelbraeht et al. (1998) to examine the dust attenuation. Bolatto et al. (2013), Leroy et al. (2015), and Meier et al. (2015) previously published analyses based on these data, but except for a brief mention of recombination lines in the latter paper, they focused on the molecular gas, whereas we will concentrate on the photoionized gas.

Radio and millimetre recombination lines have previously been detected from NGC 253 (e.g. Seaquist & Bell 1977; Mebold et al. 1980; Anantharamaiah & Goss 1996; Puxley et al. 1997; Mohan, Anantharamaiah & Goss 2002; Mohan, Goss & Anantharamaiah 2005; Rodríguez-Rico et al. 2006; Kepley et al. 2011). This includes the detection of H40 α emission by Puxley et al. (1997). However, our analysis will focus on millimetre lines that are less susceptible to masing effects than most previous recombination line observations, which have been at lower frequencies. Additionally, most of the continuum at the location of the H40 α line is free-free emission, allowing us to use the line and continuum data together to measure T_c , whereas the lower frequency data include more synchrotron emission. The ALMA data also have superior spatial resolutions, spectral resolutions, and sensitivities than most previously published NGC 253 data. This ultimately serves as an example of

^{*}E-mail: george.bendo@manchester.ac.uk

the future work on extragalactic star formation in nearby galaxies that can be done with ALMA.

2 DATA

The data were originally acquired as part of programme 2011.0.00172.S and published by Bolatto et al. (2013). The observations covering the H40 α line are from three execution blocks (EBs) performed on 2012 May 07, July 01, and July 02. Three locations along the major axis spaced by 25 arcsec were observed, and the total integration time per location was 29 min. Only 14–20 antennas were operational. The spectral window covering the H40 α line was centred at a sky frequency of 98.54 GHz, contained 3840 channels each with a width of 488 kHz (1.5 km s⁻¹), and included both polarizations. Uranus was the flux calibrator, J2333–237 was the bandpass calibrator, and J0137–245 was the phase calibrator.

We reprocessed the data using the Common Astronomy Software Applications version 4.2.2, which includes a version of the flux calibration (Butler-JPL-Horizons 2012) that is more up to date than the one used to create the data in the ALMA archive. The visibility data were processed through steps to flag bad data and to calibrate the phase and amplitude as a function of frequency and time. Next, we rescaled the amplitudes of the visibility data so that the signal measured for J0137-245 in the individual EBs matched the weighted average of these values, and then we concatenated the data. We produced two versions of the image cube (with and without continuum) using a clean algorithm with natural weightings in an interactive mode. Although the primary beam is 63 arcsec, we created image cubes covering a 32 × 32 arcsec region (with 0.1 arcsec pixels) because no detectable emission is found outside this region. The cubes used in the analysis cover a sky frequency range between 98.80 and 99.09 GHz, and each channel in each cube covers eight channels in the visibility data, which corresponds to 3.9 MHz (~11.8 km s⁻¹). For display purposes, we also produced a cube that covered 97.64-99.44 GHz, which was the full usable range of the spectral window containing the H40\alpha line, with the same spatial and spectral resolution. The full width at half-maximum (FWHM) of the reconstructed beam is 1.9×1.6 arcsec; assuming a distance of 3.44 ± 0.26 Mpc (based on the average of distances measured by Dalcanton et al. 2009), this corresponds to spatial scales of ~30 pc. The flux calibration uncertainty reported in the ALMA Technical Handbook is 5 per cent (Lundgren 2013). The 98.54 GHz

flux densities for the bandpass calibrator (1.15 \pm 0.04 Jy) and the phase calibrator (1.09 \pm 0.06 Jy) have relative uncertainties (based on the variations in measurements from individual EBs) that are consistent with the Technical Handbook, although unidentified systematic amplitude calibration effects could affect the flux densities. Cleaned image cubes of the bandpass and phase calibrators show <1 per cent variations in the flux density from channel to channel, and no spectral features are seen at the position of the H40 α line in the visibility data for the calibration sources, which indicates that any line emission >1 per cent of the continuum emission is not caused by calibration issues.

We had access to data from programme 2011.0.00061.S (PI: Takano) that also covers the H40 α line. Because the spectral settings were different from programme 2011.0.00172.S, we did not use the data in our analysis, but we did examine the processed archival data for programme 2011.0.00061.S to confirm that the H40 α emission is detected in those data.

H40\alpha fluxes, mean velocities (relative to the Solar system barycentre, and velocity FWHM were measured in the continuumsubtracted image cube, and the continuum at 99.02 GHz was measured in the other image cube by fitting and removing the line emission. Images of the continuum emission (based on all continnum data within the spectral window), the H40lpha flux, and the H40lphamean velocity are shown in Fig. 1. Spectra integrated over the central 20 × 10 arcsec as well as integrated within regions covering the three brightest regions are shown in Fig. 2. Details of the measurements in these regions are listed in Table 1. The uncertainties in the measurements incorporate the noise per channel values listed in Table 1, but except for the east (E) region, the accuracy in the continuum and H40\alpha fluxes is primarily limited by the calibration uncertainties. Most of the signal outside the 20×10 arcsec ellipse is detected at 3σ , and we also lack the un coverage to recover >20 arcsec structures.

The central star-forming region can be divided into three knots that lie along the major axis of the galaxy. The central (C) and west (W) sources are detected at >10 σ in both the continuum and H40 α emission. The eastern source is detected at >10 σ in continuum emission as well, but the peak is only detected at the ~8 σ level in H40 α emission. Although all three sources had previously been detected in radio continuum emission (Mohan et al. 2005; Kepley et al. 2011), only Anantharamaiah & Goss (1996) had previously shown radio recombination line emission from all three sources.

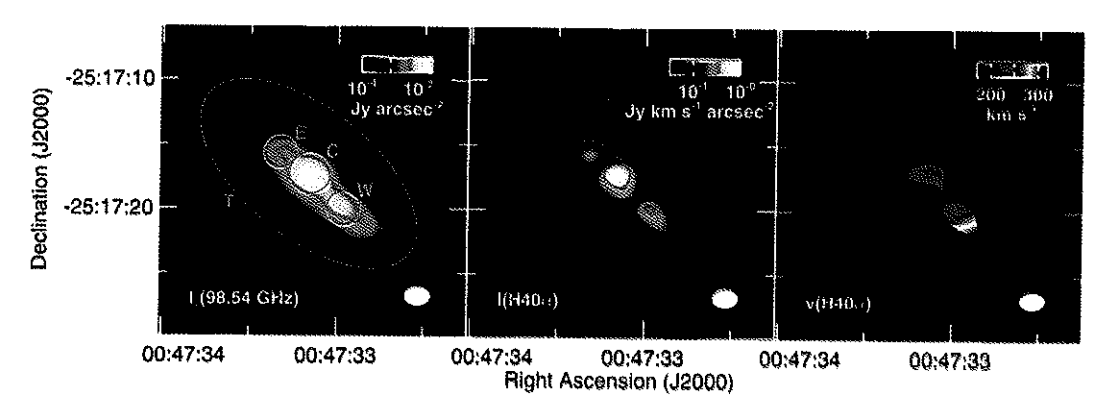


Figure 1. Images of the continuum surface brightness, the H40 α intensity, and the H40 α mean velocity in the central 32 × 32 arcsec of NGC 253. The velocity, which is relative to the Solar system barycentre, is only shown for data where the H40 α intensity is detected at the 5 α level. The white oval at the bottom right of each panel shows the FWHM of the beam. The green regions in the continuum image show the total (T), east (E), central (C), and west (W) regions within which fluxes and spectra were measured. The spectra are shown in Fig. 2, and measured quantities are listed in Table 1.

MNRASL 450, L80-L84 (2015)

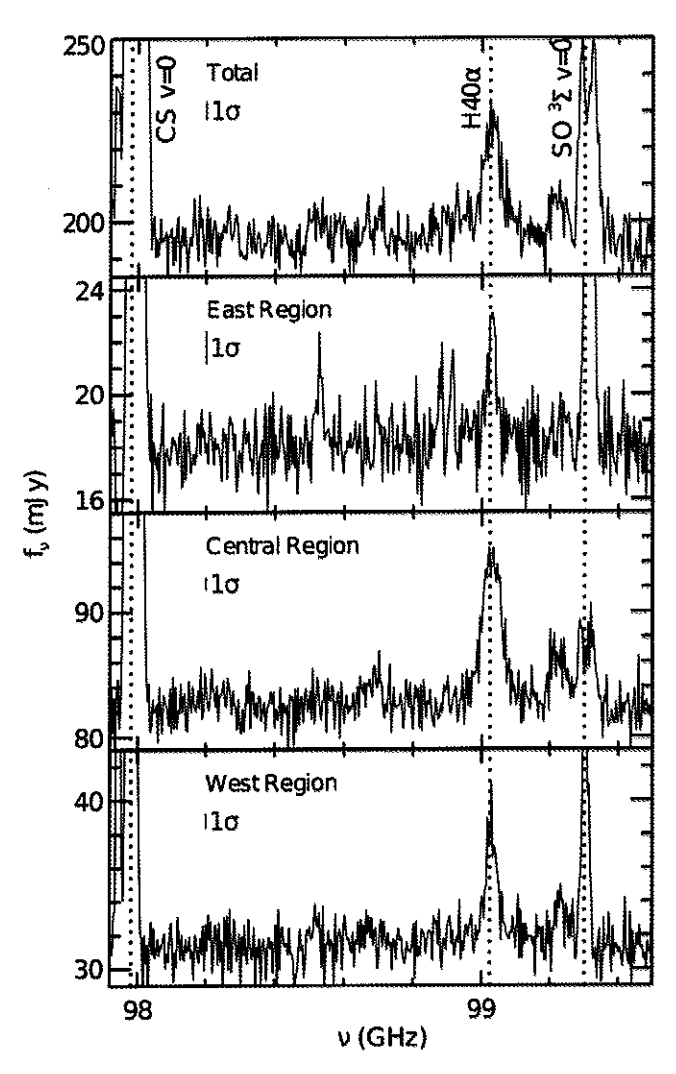


Figure 2. Plots of the spectra measured in the 20×10 arcsec elliptical region (labelled as 'Total') and in the cust, central, and west subregions identified in Fig. 1. The frequencies are rest frequencies based on the velocities in Table 1. The red lines show major spectral features identified using Speatal.orgue (http://www.cv.nrao.edu/php/splat/). The blue bar shows the noise per channel as listed in Table 1.

The same structure is also seen in the Bry image from Engelbracht et al. (1998), but the source is only marginally resolved and does not appear to show the same peak in recombination line emission.

The H40 α emission from the central source is relatively broad (with an FWHM of 191 \pm 4 km s⁻¹) and appears to be rotating

orthogonally to the plane of the galaxy, which is consistent with previous radio recombination line observations (Anantharamaiah & Goss 1996; Rodríguez-Rico et al. 2006; Kepley et al. 2011). This may indicate that material has recently fallen into the central region, that the central source comprises two superimposed photoionized regions, or that the ionized gas is in a superwind that is flowing in a direction aligned with the minor axis. It is unlikely that an active galactic nucleus is present, as the H40 α line would appear

* 1000 km s ⁻¹ in width. We do not detect any asymmetry in the line emission from the central source as had been reported in some prior recombination line observations (Mohan et al. 2002; Kepley et al. 2011) but not others. The reason for this discrepancy is unclear, although one possibility is that the line shapes differ because the lower frequency lines are probing less dense gas than the H40\alpha line.

3 ANALYSIS

For determining the relative contribution of free-free emission to the 99.02 GHz continuum, the frequency coverage of the ALMA data by itself is insufficient for modelling the spectral energy distribution. Peel et al. (2011) indicate that most of the globally integrated 99.02 GHz emission would be continuum. However, Rodríguez-Rico et al. (2006) found a much smaller contribution of free-free emission to the central 30 arcsec, but they assumed that the slope of the synchrotron emission is fixed by the 5 and 15 GHz data points. If we instead repeat this fit but allow the slope of the synchrotron component to vary, as shown in Fig. 3, we find that 70 ± 10 per cent of the 99.02 GHz emission is from free-free emission. We applied this correction to the measured continuum emission in the rest of our analysis.

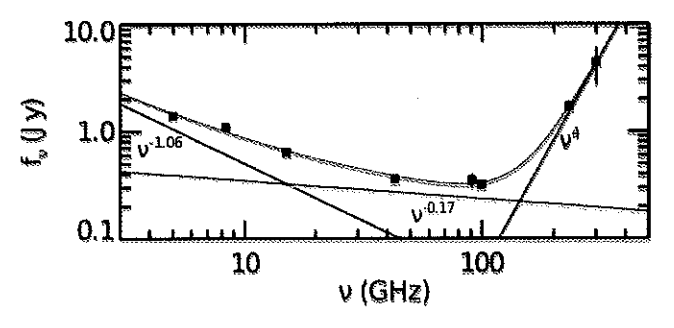


Figure 3. The spectral energy distribution of the central 30 aresec of NGC 253 based on the data from Rodríguez-Rico et al. (2006). The dark grey lines shows the function fit to the data, which comprises a synchrotron function with a power-law index that was allowed to vary (shown in red), a free-free function that scales as $v^{-0.17}$ (shown in green), and a mostified Rayleigh-Jeans function for dust that varies as v^{2} (shown in blue).

Table 1. Measurements of the continuum and H40\alpha emission.

Region	egion Noise per channel ^a (mJy)	Free-free flux Flux density ^b	H40œ	H40a		H40\alpha /Free-free ratio ^b (km s ⁻¹)	Electron temperature ⁶ (K)	SFR	
			Flux	Mean velocity (km s ⁻¹)				Free-free ^h (M⊙ yr ¹)	(M@ yr 1)
			(Jy km s ⁻¹)						
Total	5.2	146.5 ± 17.2	6,91 ± 0,80	232 ± 2	169 ± 10	47.2 ± 2.4	3900 ± 300	1,59 ± 0.16	1.87 ± 0.18
East	1.3	13.4 ± 1.5	0.64 ± 0.08	206 ± 4	85 ± 11	48.0 ± 3.3	3900 ± 400	0.15 ± 0.02	-0.17 ± 0.02
Central	1.0	58.6 ± 7.0	2.49 ± 0.28	224 未 2	191 素 5	42.5 ± 2.0	4500 ± 300	0.58 ± 0.05	0.63 ± 0.06
West	0.9	22.8 ± 2.7	1.13 ± 0.15	246 ± 1	H3 ± 8	49.5 素 4.1	3700 ± 400	0.25 ± 0.03	0.29 ± 0.02

The root mean square noise levels were measured on either side of the H40 α line at rest frequencies (based on v=224 km s⁻¹) of 98.880–98.920 and 99.135–99.175 GHz (excluding the unidentified spectral feature at 98.915 GHz in the east region). These numbers are based on multiplying the measured continuum by 0.70 \pm 0.10 to account for emission from sources other than free-free emission.

The ratio of the H40 α flux density f_{ν} (line) integrated over velocity ν to the free-free flux density f_{ν} (cont) can be written as

$$\frac{f_{\nu}(\text{line}) \, d\nu}{f_{\nu}(\text{cont})} = \frac{Jy}{Jy \, \text{km s}^{-1}}$$

$$= 5.06 \times 10^{32} = \frac{\epsilon_{\nu}}{\text{erg s}^{-1} \, \text{cm}^{-3}} = \frac{\nu}{\text{GHz}} = \frac{7.83}{K} = \frac{T_{e}}{K} = 0.5$$
(1)

based on equations from Scoville & Murchikova (2013). The emissivity ϵ_{ν} varies slowly as a function of electron density n_{ν} but varies strongly with T_c . As shown in Table 1, we measure lineto-continuum ratios of 42.5 in the central region and ~50 in the east and west regions. We used these ratios and interpolated between the e, values from Storey & Hummer (1995) for case B recombination and $n_e = 10^3$ cm⁻³ to calculate T_e for each of the regions in our analysis. The T_c values of 3700-4500 K we measure are slightly lower than the previously reported values from Puxley et al. (1997) and Rodríguez-Rico et al. (2006), but only by 1σ . The T_c values are also comparable with values measured by Shaver et al. (1983) and Paladini, Davies & DeZotti (2004) within the central 8 kpc of the Milky Way. If we did not apply the correction of 0.70 to the continuum emission, the measured $T_{\rm e}$ would increase to values of 5800-7100 K, which are still consistent with Milky Way values. If 50 per cent of the continuum emission is free-free, then the resulting T_e fall within the implausible range of 2500-3000 K.

The SFR that we calculate depends upon both T_c and the star formation history. The presence of both photoionized gas and supernovae (e.g. Lenc & Tingay 2006; Rampadarath et al. 2014) imply that the star formation is continuous and has been ongoing for >5 Myr. We used version 7.0.1 of the starburst99 models (Leitherer et al. 1999) to determine how to convert the number of ionizing photons produced as a function of time (Q) to SFR. This version of starburst99 incorporates versions of the Geneva stellar evolution tracks that include rotation, with the rotation velocities of zero rotation and 40 per cent of the break-up velocity representing two potential extremes (Leitherer et al. 2014). Using the average of the results from these two versions of the Geneva tracks for Z = 0.040 metallicity (the highest metallicity for which tracks are available) and a Kroupa (2002) initial mass function for a mass range of $0.1-100 \,\mathrm{M}_{\odot}$, we find that SFR = $1 \,\mathrm{M}_{\odot}$ yr 1 corresponds to $Q = 1.85 \times 10^{53}$ s⁻¹ after ~5 Myr of continuous star formation.1

Given this, SFR can be calculated from either the free-free or recombination line emission using

$$\frac{\text{SFR(line)}}{\text{M}_{\odot} \text{ yr}^{-1}} = 2.16 \times 10^{-23} \frac{\alpha_B \text{ cm}^6}{\epsilon_v \text{ erg}}$$

$$\times \frac{\nu}{\text{GHz}} \frac{D}{\text{Mpc}}^2 \frac{f_v(\text{line}) \text{ d}v}{\text{Jy km s}^{-1}}$$
(2)

¹ The Q from the two rotation scenarios differ by a factor of \sim 1.8. Using Z=0.014 metallicity (the next lower metallicity for which Geneva tracks are available) had a <5 per cent effect on the results. Using older stellar population models that did not include stellar rotation, Kennicutt (1998) reported a conversion factor that would increase SFR by a factor of \sim 2, and Murphy et al. (2011) gave a conversion factor that would increase SFR by 35 per cent.

and
$$\frac{\text{SFR(cont)}}{\text{M}_{\odot} \text{ yr}^{-1}} = 1.09 \times 10^{10} \frac{\alpha_{H}}{\text{cm}^{3} \text{ s}^{-1}}$$

$$\times \frac{\nu}{\text{GHz}} = \frac{0.17}{\text{K}} \frac{T_{c}}{\text{Mpc}} \frac{0.5}{\text{Mpc}} \frac{D}{\text{Jy}}^{-2} \frac{f_{c}(\text{cont})}{\text{Jy}} . (3)$$

which are adapted from Scoville & Murchikova (2013). The α_B term, which is the effective recombination coefficient listed by Storey & Hummer (1995), varies by a factor of ~3 between 5000 and 15 000 K but negligibly with electron density within the range 10^2 – 10^5 cm 3 . The SFRs listed in Table 1 are based on α_B calculated using $n_c=10^3$ cm 3 . The two SFRs, which are mathematically linked through equation (1), are limited by both the photometric accuracy and the assumptions behind the conversion between Q and SFR. Because we are adjusting T_c based on the line-to-continuum ratio, the calculated SFR from the continua vary by $\ll 1\sigma$ if we do not adjust the continuum emission to account for emission sources other than free--free emission.

A comparison of these results to SFRs from ultraviolet, optical, or near-infrared data would not be worthwhile, as the nuclear region is heavily obscured at those wavelengths (as discussed below). The mid- and far-infrared continuum emission tends to be either poorly resolved or saturated in most existing data, making it impossible to calculate SFRs from dust emission on spatial scales comparable to the ALMA data. However, we can compare our total SFR (and Q, which is $(3.2 \pm 0.2) \times 10^{83} \, \mathrm{s}^{-1}$ within the central 20×10 arcsec) to equivalent measurements that have been made using millimetre and radio data (after rescaling all SFR and Q to correspond to distances of 3.44 Mpc).

Puxley et al. (1997) obtained a distance-adjusted Q of $(7.0 \pm 1.5) \times 10^{53}$ s⁻¹ from H40 α data that is significantly higher than our Q or other measurements of Q, but the line is detected at the $\sim 5\sigma$ level, which may indicate issues with the reliability of their data. Rodríguez-Rico et al. (2006) and Kepley et al. (2011) report Q based on lower frequency recombination line data that are ~3 x lower than our measurement. This could be related to sensi. tivity issues since they had difficulty detecting line emission from all three sources that we detected. However, these groups may be probing primarily lower density gas in the lower frequency data. which would lead to lower estimates of Q than what we obtain with H40α, Rampadarath et al. (2014), in the latest 2.3 GHz analysis of supernova remnants in NGC 253, measure an SFR upper limit of 4.9 M_O yr⁻¹; our SFR falls below this limit. Off et al. (2005) measured a distance-adjusted SFR of 4.9 ± 0.5 M_☉ yr⁻¹ from 25 GHz continuum data which is ~3 × higher than our value, but they rely upon a formula originating from Condon (1992) that uses a conversion of synchrotron emission to SFR may need to be recalibrated. Rodríguez-Rico et al. (2006) also produced an estimate of Q based on the continuum emission that is $\sim 3 \times$ lower than our value, but as we indicated above, they may have biased the free-free emission estimates to low values.

The optical recombination line emission from the centre of NGC 253 is heavily obscured, but Engelbracht et al. (1998) measured multiple near-infrared recombination lines, including $Pa\beta$ and $Br\gamma$, that can be compared to H40 α emission to infer the dust attenuation to the nucleus. If we assume that the dust functions like an attenuating sheet, then the dust attenuation A_{λ} at a given infrared wavelength λ is related to the ratio of the infrared line flux $f(\lambda)$ to the H40 α line flux $f(H40\alpha)$ by

$$A_{\lambda} = -1.086 \ln^{\frac{\lambda}{2}} \frac{\epsilon_{H4\lambda_{\lambda}}}{\epsilon_{\lambda}} \frac{3027 \, \mu m}{\lambda} \frac{f(\lambda)}{f(H40\alpha)} \stackrel{?}{\sim} (4)$$

The Engelbracht et al. (1998) spectroscopy data were acquired within a 12×2.4 arcsec aperture that also contains ~ 70 per cent of the H40 α emission in our data, so we compare the Pa β and Bry fluxes from the Engelbracht et al. (1998) spectroscopy data (which were the lines detected at the highest signal-to-noise levels) to $0.7 \times$ our total H40 α flux. Assuming that $n_c = 10^3$ cm⁻³ and using $T_c = 3900 \pm 300$ K from Table 1, we obtain $A_{Pa\beta} = 5.0 \pm 0.2$ and $A_{Bry} = 4.2 \pm 0.2$. This is higher than the values of $A_J = 2.00 \pm 0.36$ and $A_K = 0.87 \pm 0.16$ for an attenuating sheet as reported by Engelbracht et al. (1998). The results are affected by the assumed n_c , although the effects are of the order of 0.2 dex for a range of 10^2-10^5 cm⁻³.

It is likely that the attenuation was underestimated by Engelbracht et al. (1998). In their Br γ image, they do not detect the same central peak that we detect in H40 α (although this may be attributable to a coarser spatial resolution in the Br γ data), and they measure a lower velocity dispersion than we do, implying that the emission from the central region is heavily obscured in the infrared data. Engelbracht et al. (1998) indicate that the dust attenuation may be better described by a clumpy medium, which could affect the attenuation results. While it is beyond the scope of this paper to explore a more complex treatment of the attenuating medium, the comparison of A_{λ} values based on the attenuating sheet scenario still suggests that the attenuation measured by Engelbracht et al. (1998) is too low by \sim 3 dex.

The broader implication of these result is that near-infrared recombination line emission is more heavily obscured in very dusty galaxies, including starbursts like NGC 253 as well as luminous and ultraluminous infrared galaxies (galaxies with infrared luminosities $>\!10^{11}$ L_{\odot}), than previously thought. SFRs based on near-infrared data may be underestimated in such objects. Near-infrared recombination line emission has been used to calibrate some SFR calculations based on combining ultraviolet/optical star formation tracers with mid-infrared star formation tracers (e.g. Calzetti et al. 2007). While these formulae are probably still accurate for many galaxies, these equations may need to be recalibrated for application to more dusty objects.

4 SUMMARY AND CONCLUSIONS

Using ALMA observations of free-free and H40 α emission at 99.02 GHz from the centre of NGC 253, we obtain the following key results.

- (i) We measure $T_{\rm e}$ of 3700-4500 K within the detected regions in the centre of the galaxy, which matches previous measurements within NGC 253 as is consistent with the range of values seen in the inner 8 kpc of the Milky Way.
- (ii) Using both the continuum and line emission, we measure a Q of $(3.2 \pm 0.2) \times 10^{53} \, \mathrm{s}^{-1}$ and an SFR of $1.73 \pm 0.12 \, \mathrm{M}_{\odot}$ yr⁻¹ for the central 20×10 arcsec. This measurement falls within the range of previously published millimetre and radio results, which are inconsistent with each other, although our recombination line emission is detected at superior sensitivity levels, and our constraints on the relative contribution of free-free emission at millimetre wavelengths are more reliable.
- (iii) The ratio of H40 α emission to the near-infrared line emission reported by Engelbracht et al. (1998) implies that the central region is obscured by \sim 3 dex more than originally inferred. Given this, near-infrared line emission should be used with caution to measure SFR in very dusty regions or to calibrate other SFR metrics.

This analysis represents a sample of what can potentially be achieved using ALMA to measure T_e and SFR. While this analysis

is based on a target where millimetre and radio recombination line emission has been detected before, it is also based on data from ALMA Cycle 0 in which approximately one-third of the ALMA antennas were operational. Data from dedicated observations using ALMA when it is fully operational can potentially uncover millimetre recombination line emission in more galaxies, allowing us to probe star formation in sources where other data are not usable or to calibrate other SFR metrics.

ACKNOWLEDGEMENTS

We thank the reviewer for the useful comments on this paper. GJB, RJB, GAF, and TWMB acknowledge support from STFC Grant ST/M000982/1, CD acknowledges support from STFC Grant ST/L000768/1 and ERC Starting (Consolidator) Grant no. 307209. This paper makes use of the following ALMA data: ADS/JAO.ALMA#2011.0.00172.S. ALMA is a partnership of ESO (representing its member states). NSF (USA) and NINS (Japan), together with NRC (Canada) and NSC and ASIAA (Taiwan), in cooperation with the Republic of Chile. The Joint ALMA Observatory is operated by ESO, AUI/NRAO and NAOJ.

REFERENCES

Anantharamaiah K. R., Goss W. M., 1996, ApJ, 466, L13

Bolatto A. D. et al., 2013, Nature, 499, 450

Calzetti D. et al., 2007, ApJ, 666, 870

Calzetti D., Sheth K., Churchwell E., Jackson J., 2009, in Sheth K., Noriega-Crespo A., Ingalls J., Paladini R., eds, The Evolving 18M in the Milky Way and Nearby Galaxies. Spitzer Science Center, Pasadena, CA, p. E8 Condon J. J., 1992, ARA&A, 30, 575

Dalcanton J. J. et al., 2009, ApJS, 183, 67

Engelbracht C. W., Ricke M. J., Ricke G. H., Kelly D. M., Achtermann J. M., 1998, ApJ, 505, 639

Gordon M. A., Walmsley C. M., 1990, ApJ, 365, 606

Kennicutt R. C., Jr. 1998, ARA&A, 36, 189

Keptey A. A., Chomiuk L., Johnson K. E., Goss W. M., Balser D. S., Pisano D. J., 2011, ApJ, 739, L24

Kroupa P., 2002, Science, 295, 82

Leitherer C. et al., 1999, ApJS, 123, 3

Leitherer C., Ekström S., Meynet G., Schaerer D., Agienko K. B., Levesque E. M., 2014, ApJS, 212, 14

Lene E., Tingay S. J., 2006, AJ, 132, 1333

Leroy A. K. et al., 2015, ApJ, 801, 25

Lundgren A., 2013, ALMA Cycle 2 Technical Hundbook Version 1.1. ALMA, Santiago

Mebold U., Shaver P. A., Bell M. B., Scaquist E. R., 1980, A&A, 82, 272 Meter D. S. et al., 2015, ApJ, 801, 63

Mohan N. R., Ananthuramaiah K. R., Goss W. M., 2002, ApJ, 574, 701

Mohan N. R., Goss W. M., Anantharamaiah K. R., 2005, A&A, 432, 1

Murphy E. J. et al., 2011, ApJ, 737, 67

On J., Weiss A., Henkel C., Walter F., 2005, ApJ, 629, 767

Paludini R., Davies R. D., DeZoni G., 2004, MNRAS, 347, 237

Peel M. W., Dickinson C., Davies R. D., Clements D. L., Beswick R. J., 2011, MNRAS, 416, L99

Puxley P. J., Mountain C. M., Brund P. W. J. L., Moore T. J. T., Nukai N., 1997, ApJ, 485, 143

Rampadarath H., Morgan J. S., Lenc E., Tingay S. J., 2014, AJ, 147, 5

Rodríguez-Rico C. A., Goss W. M., Zhao J.-H., Gómez Y., Anantharamaiah K. R., 2006, ApJ, 644, 914

Scoville N., Murchikova L., 2013, ApJ, 779, 75

Seaquist E. R., Bell M. B., 1977, A&A, 60, L1

Shaver P. A., McGee R. X., Newton L. M., Danks A. C., Pottasch S. R., 1983, MNRAS, 204, 53

Storey P. J., Hummer D. G., 1995, MNRAS, 272, 41

This paper has been typeset from a TEXAMEN file prepared by the author.